

# SRTFD: Scalable Real-Time Fault Diagnosis through Online Continual Learning

Dandan Zhao  
Chongqing University  
Chongqing, China  
Nanyang Technological University  
Singapore  
whsmhgy@gmail.com

Karthick Sharma  
University of Sri Jayewardenepura  
Doimukh, Arunachal Pradesh, Sri  
Lanka  
en93899@sjp.ac.lk

Hongpeng Yin  
Chongqing University  
Chongqing, China  
yinhongpeng@cqu.edu.cn

Yuxin Qi  
Shanghai Jiao Tong University  
Shanghai, Beijing Shi, China  
qiyuxin98@sjtu.edu.cn

Shuhao Zhang  
Nanyang Technological University  
Singapore  
shuhao.zhang@ntu.edu.sg

## ABSTRACT

Fault diagnosis (FD) is essential for maintaining operational safety and minimizing economic losses by detecting system abnormalities. Recently, deep learning (DL)-driven FD methods have gained prominence, offering significant improvements in precision and adaptability through the utilization of extensive datasets and advanced DL models. Modern industrial environments, however, demand FD methods that can handle new fault types, dynamic conditions, large-scale data, and provide real-time responses with minimal prior information. Although online continual learning (OCL) demonstrates potential in addressing these requirements by enabling DL models to continuously learn from streaming data, it faces challenges such as data redundancy, imbalance, and limited labeled data. To overcome these limitations, we propose SRTFD, a scalable real-time fault diagnosis framework that enhances OCL with three critical methods: *Retrospect Coreset Selection (RCS)*, which selects the most relevant data to reduce redundant training and improve efficiency; *Global Balance Technique (GBT)*, which ensures balanced coreset selection and robust model performance; and *Confidence and Uncertainty-driven Pseudo-label Learning (CUPL)*, which updates the model using unlabeled data for continuous adaptation. Extensive experiments on a real-world dataset and two public simulated datasets demonstrate SRTFD's effectiveness and potential for providing advanced, scalable, and precise fault diagnosis in modern industrial systems.

## KEYWORDS

Fault diagnosis, Online continual learning

## ACM Reference Format:

Dandan Zhao, Karthick Sharma, Hongpeng Yin, Yuxin Qi, and Shuhao Zhang. 2018. SRTFD: Scalable Real-Time Fault Diagnosis through Online Continual Learning. In *Proceedings of Make sure to enter the correct conference title from your rights confirmation email (Conference acronym 'XX)*. ACM, New York, NY, USA, 13 pages. <https://doi.org/XXXXXXX.XXXXXXX>

## 1 INTRODUCTION

Faults in engineering systems pose substantial risks to both performance and safety [29]. For instance, faults in steel hot rolling processes can lead to defective steel slabs, resulting in significant scrap losses and compromising worker safety. Similarly, faults in autonomous vehicles can cause navigation errors or system malfunctions, potentially leading to accidents and endangering passengers and pedestrians. Consequently, fault diagnosis (FD) – the process of detecting and identifying potential faults within these systems – is crucial for maintaining reliability, safety, and economic efficiency [1]. While recent research in computer vision has focused on industrial anomaly detection (IAD) [4, 10, 14, 15, 35], primarily addressing quality faults in end products using image data to identify statistical features and pattern changes, FD targets process faults. FD is essential for immediate fault detection and intervention, focusing on specific functional problems using sensor data to prevent system failures.

FD techniques have evolved significantly over time. In the 19th century, FD began with basic limit checking and progressed to model-based FD, which involves physically modeling the entire industrial system's working process and incorporating statistical methods such as trend analysis and parameter estimation [16]. The evolution continued with the development of knowledge-based FD, which utilizes signal models and spectral analysis [27]. The advent of artificial intelligence and neural networks marked a new era of data-driven FD [8, 37]. Today, the explosion of data has further propelled the development of deep learning (DL)-driven FD methods. By leveraging large datasets and sophisticated DL models, these methods have significantly enhanced the precision and adaptability of FD, making them crucial for modern industrial environments [9]. Our work builds on this progression, aiming to address the challenges of real-time fault diagnosis in dynamic and large-scale systems with DL-driven FD methods.

Permission to make digital or hard copies of all or part of this work for personal or classroom use is granted without fee provided that copies are not made or distributed for profit or commercial advantage and that copies bear this notice and the full citation on the first page. Copyrights for components of this work owned by others than the author(s) must be honored. Abstracting with credit is permitted. To copy otherwise, or republish, to post on servers or to redistribute to lists, requires prior specific permission and/or a fee. Request permissions from [permissions@acm.org](mailto:permissions@acm.org).  
Conference acronym 'XX, June 03–05, 2018, Woodstock, NY

© 2018 Copyright held by the owner/author(s). Publication rights licensed to ACM.  
ACM ISBN 978-1-4503-XXXX-X/18/06...\$15.00  
<https://doi.org/XXXXXXX.XXXXXXX>

**Table 1: The existing state-of-the-art FD methods and the key challenges in modern FD tasks.**

Methods	Year	Key Challenges				
		Low-training cost	High-data efficiency	Large-scale data	Imbalance data	Limited labeled data
OSELM [19]	2020	×	×	×	✓	×
D-CART [11]	2020	✓	×	×	×	×
TCNN [38]	2020	✓	×	×	×	×
OSSBLs [28]	2021	×	×	×	×	✓
AMPNet [15]	2022	×	×	✓	×	×
1D-CNN [13]	2022	×	×	×	×	✓
TVOTL [40]	2023	×	×	×	×	✓
ODDFD [20]	2023	×	×	×	×	✓
ODCT [23]	2024	×	×	×	✓	×
OLFA [39]	2024	×	×	×	×	✓
MPOS-RVFL [18]	2024	✓	×	×	✓	✓
SRTFD (Ours)	2024	✓	✓	✓	✓	✓

Today, as equipment and systems become increasingly complex, refined, large-scale, and digitalized, the demands for modern FD methods have evolved significantly [41]. Modern industrial environments require FD methods that can handle new fault types, adapt to changing conditions, process large-scale data efficiently, provide real-time responses, and operate with minimal prior information [18]. These requirements present several key technical challenges, including managing training costs, ensuring data efficiency, processing large-scale data, handling data imbalance, and working with limited labeled data. Furthermore, the continuous and dynamic nature of industrial processes necessitates handling streaming data and maintaining model performance over time. Existing DL-based FD methods often struggle with these challenges, as summarized in Table 1. They particularly face issues related to high computational costs, inefficiencies in handling streaming data, and difficulties in sustaining model performance due to data redundancy and imbalance. This underscores the necessity for more advanced and integrated FD techniques that can meet the evolving needs of modern industrial systems.

Online continual learning (OCL) [17] offers a promising solution to the limitations of traditional DL-based FD methods by enabling models to continuously learn from streaming data. This capability is crucial for adapting to new fault types, changing operating conditions, and meeting real-time requirements. Recent advancements in OCL, such as CAMEL [22] and GoodCore [5], have focused on reducing training costs and improving data efficiency. However, directly applying these OCL approaches to fault diagnosis is not straightforward due to domain-specific challenges including 1) highly redundant system monitoring data, 2) extreme data imbalance, and 3) the difficulty of collecting sufficient labeled samples. Therefore, while OCL provides a robust framework, it requires significant adaptation to effectively meet the unique demands of real-time fault diagnosis in modern industrial environments.

To address the limitations of traditional and OCL-based fault diagnosis methods, we propose SRTFD, a scalable real-time fault diagnosis framework composed of three key components: Retrospect Coreset Selection (RCS), Global Balance Technique (GBT), and Confidence and Uncertainty-driven Pseudo-label Learning (CUPL). RCS enhances data efficiency and reduces training costs by selecting the most relevant data for model updates, thus avoiding redundant training on unnecessary monitoring data. GBT tackles data

imbalance by ensuring balanced coreset selection and maintaining robust model performance. CUPL enables model updates using unlabeled data, addressing the scarcity of labeled monitoring data and facilitating continuous adaptation. By integrating these components, SRTFD effectively handles the complexities of real-time fault diagnosis in modern industrial environments, characterized by large-scale, streaming, and unbalanced data with minimal labeled samples.

We validated the effectiveness of SRTFD through experiments on one real-world industrial process (Hot Roll of Steel, HRS) and two simulation processes (Tennessee Eastman Process, TEP, and CAR Learning to Act, CARLA). The HRS dataset includes motor current data from 294 rollers across five fault categories, characterized by high imbalance and limited samples. The TEP dataset has 21 fault categories, and the CARLA dataset includes single-sensor and multi-sensor faults under three weather conditions, simulating real-world variability. We compared SRTFD against five benchmarks: a baseline experience replay (ER) model [7], CAMEL [22], ASER [34], AGEM [24], and MPOS-RVFL [18], focusing on class-incremental learning and varying working conditions. Our approach showed superior performance and efficiency, with improvements of 2.73% in recall, 1.43% in precision, 1.76% in F1 score, 1.81% in G-means, and a 55.83% reduction in training time compared to state-of-the-art FD and OCL methods. These results underscore the effectiveness and cost-efficiency of SRTFD for industrial applications.

The main contributions of this work are:

- We propose SRTFD<sup>1</sup>, a novel and scalable real-time fault diagnosis framework designed to enhance online continual learning (OCL) for industrial applications. This framework effectively addresses the limitations of existing fault diagnosis methods, particularly in handling large-scale, streaming, and imbalanced data with minimal labeled samples.
- SRTFD integrates three innovative components: Retrospect Coreset Selection (RCS) to enhance data efficiency and reduce training costs, Global Balance Technique (GBT) to tackle data imbalance and maintain robust model performance, and Confidence and Uncertainty-driven Pseudo-label Learning (CUPL) to enable continuous model updates using unlabeled data.
- We validate SRTFD through extensive experiments on real-world and simulated datasets, demonstrating superior performance and efficiency compared to state-of-the-art methods. Our approach achieved notable improvements in recall, precision, F1 score, G-means, and training time, underscoring its effectiveness and cost-efficiency for real-time fault diagnosis in modern industrial environments.

## 2 BACKGROUND AND MOTIVATION

### 2.1 Traditional Data-driven-based FD

Traditional data-driven FD involves three steps: data collection, model training, and fault prediction. Let  $X^{tr} = \{x_1^{tr}, x_2^{tr}, \dots, x_{n_{tr}}^{tr}\}$  and  $X^{te} = \{x_1^{te}, x_2^{te}, \dots, x_{n_{te}}^{te}\}$  be the training and testing samples, respectively. Corresponding labels are  $Y^{tr} = \{y_1^{tr}, y_2^{tr}, \dots, y_{n_{tr}}^{tr}\}$  and  $Y^{te} = \{y_1^{te}, y_2^{te}, \dots, y_{n_{te}}^{te}\}$ , with  $n_{tr}$  and  $n_{te}$  being the number

<sup>1</sup>Our code and public datasets are available at: <https://anonymous.open.science/status/SRTFD-F813>

of samples. Labels range from 0 to  $c$ , where 0 indicates normal samples and 1 to  $c$  denote different fault categories, with  $c$  being the total number of fault categories.

Features of collected samples are extracted by  $\phi(\cdot)$  before model training. The FD model is then trained using the following loss function:

$$\min \sum_{i=1}^{n_{tr}} \mathcal{L}(f(\phi(x_i^{tr}); \theta), y_i^{tr}), \quad (1)$$

where,  $\theta$  denotes the model parameters,  $x_i^{tr}$  is the  $i$ -th training sample ( $i = 1, 2, \dots, n_{tr}$ ). For a new test sample  $x_j^{te}$  ( $j = 1, 2, \dots, n_{te}$ ), the corresponding label  $y_j^{te}$  can be predicted by the trained FD model as follows:

$$\hat{y}_j^{te} = f(\phi(x_j^{te}); \theta). \quad (2)$$

Equations (1) and (2) show that fault diagnosis performance depends on the dataset quality. As monitoring data evolves, the model's performance degrades, necessitating data recollection and model retraining. This highlights a key limitation of traditional fault diagnosis methods in meeting real-world demands.

## 2.2 Online Continuous Learning

OCL [17] may address several limitations of traditional FD by enabling models to learn incrementally from streaming data. In OCL, monitoring data is collected over time as  $X^t \in \mathbb{R}^{d \times n} = \{x_1^t, x_2^t, \dots, x_n^t\}$  and  $Y^t \in \mathbb{R}^{1 \times n} = \{y_1^t, y_2^t, \dots, y_n^t\}$ , where  $d$  is the sample dimension,  $n$  is the number of samples, and  $t$  is the collection time. Thus, the loss function equation (1) becomes:

$$\min \sum_{i=1}^n \mathcal{L}(f(\phi(x_i^t); \theta_t), y_i^t), \quad (3)$$

where,  $x_i^t \in X^t$ ,  $y_i^t \in Y^t$ , and  $\theta_t$  are updated continuously as new data arrives. To update the model at time  $t$  without losing previous information,  $\theta_t$  is adjusted based on  $\theta_{t-1}$  and the loss function gradient. For models optimized by stochastic gradient descent (SGD) [31], the update rule is:

$$\theta_t \leftarrow \theta_{t-1} - \eta \frac{1}{n} \sum_{i=1}^n w_i^t \nabla \mathcal{L}(f(\phi(x_i^t); \theta_{t-1}), y_i^t), \quad (4)$$

where,  $\eta$  is the learning rate and  $w_i$  is the weight of data ( $x_i^t, y_i^t$ ). Typically,  $w_i^t = 1$  for all  $i \in [n]$ , assuming all samples are equally important. This continuous learning process allows the model to adapt to new fault classes and variable working conditions without retraining from scratch.

Although OCL addresses evolving monitoring data, it has a critical drawback: high model update costs when the data volume at time  $t$  is large. *Coreset selection* [22] mitigates this by selecting a smaller representative subset from the current batch, reducing data volume and computational requirements. This approach lowers training complexity, allowing fault diagnosis systems to efficiently manage large datasets and enhancing the scalability and performance of OCL models.

## 2.3 Motivation

Developing a robust FD framework using OCL and coreset selection is promising but faces challenges due to the unique characteristics of industrial monitoring data.

- **Redundancy:** Monitoring data is highly redundant, making OCL methods inefficient for model updates. Coreset selection within each batch overlooks global information, leading to unnecessary updates and extra training costs when consecutive batches are similar.
- **Data Imbalance:** FD data is imbalanced, with more normal operating data than fault data, and varying frequencies of different faults. This imbalance results in an unbalanced coreset, reducing FD system performance and reliability.
- **Labeled Data Scarcity:** Collecting labeled monitoring data is challenging due to the time-consuming and labor-intensive nature of manual labeling. The lack of labeled data makes model updating difficult.

To address these challenges, we propose SRTFD, a scalable real-time fault diagnosis method through OCL. The details of this approach will be introduced in the next section.

## 3 PROBLEM STATEMENT

Achieving a realistic fault diagnosis framework in complex systems is challenging due to several key issues mentioned in the previous section. These problems are formulated in this section.

Let  $D^0 = (X^0, Y^0)$  represent the data used for model pre-training, and  $X_u^t$  denote the arriving unlabeled data. The pseudo-labels  $Y_u^t$  for  $X_u^t$  can be predicted by well-trained model  $f_{\theta_t}(\cdot)$ . To handle the large-scale data that accumulates over time  $t$ , a small subset  $S^t = (Z^t, V^t)$  is selected from the pseudo-labeled samples  $U_u^t = (X_u^t, Y_u^t)$ . The semi-supervised learning strategy is employed by incorporating a small amount of labeled data  $D^t = (X^t, Y^t)$  to update the model along with the pseudo-labeled samples. Thus, the loss function at time  $t$  becomes:

$$\min \sum_{i=1}^n \mathcal{L}(f(\phi(x_i^t); \theta_t), y_i^t) + \sum_{j=1}^s \mathcal{L}(f(\phi(z_j^t); \theta_t), v_j^t), \quad (5)$$

where  $z_j^t \in Z^t$ ,  $v_j^t \in V^t$ , and  $s$  denotes the total number of samples in the subset  $S^t$ . The model parameter update rule becomes:

$$\begin{aligned} \theta_t &\leftarrow \theta_{t-1} - \eta(A + B), \\ A &= \frac{1}{n} \sum_{i=1}^n w_i^t \nabla \mathcal{L}(f(\phi(x_i^t); \theta_{t-1}), y_i^t), \\ B &= \frac{1}{s} \sum_{j=1}^s w_j^t \nabla \mathcal{L}(f(\phi(z_j^t); \theta_{t-1}), v_j^t), \end{aligned} \quad (6)$$

where,  $w_i^t$  and  $w_j^t$  are the weights of the labeled and pseudo-labeled samples, respectively, and  $\eta$  is the learning rate. The buffer  $B^t$  is crucial in OCL to avoid catastrophic forgetting. It contains data from the pseudo-labeled dataset  $S^t$  and the labeled dataset  $D^t$ , formulated as  $B^t \subseteq (S_u^t \cup D^t)$ . This allows the model to review and learn from past data while updating with new information.

The goal of SRTFD is to select an effective coreset from the current batch of data while considering historical data. First, the coreset must effectively represent the current batch of data. Thus, we have:

$$\min \left[ \sum_{j=1}^s \mathcal{L}(f(\phi(z_j^t); \theta_t), v_j^t) - \sum_{k=1}^u \mathcal{L}(f(\phi(x_k^t); \theta_t), y_k^t) \right]. \quad (7)$$

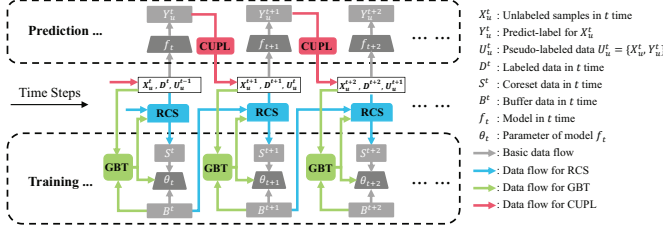


**Figure 1: SRTFD framework conducts fault diagnosis in two stages: Prediction and Training. In the Prediction stage, unlabeled samples are pseudo-labeled and combined with labeled data for model updates via CUPL. In the Training stage, the model is iteratively trained using RCS and GBT to ensure effective learning despite class imbalances.**

However, the coreset from the above objective function only considers the current batch. To account for historical data, the selected coreset at each time step should not overlap with previous coresets. For the entire coreset  $S^T$ ,  $T = 1, 2, \dots, t-1$ , it should meet the condition  $S^t \cap S^T = \emptyset$ . Additionally, to address the internal imbalance, the proportion of samples from each class in the coreset should be equal. If there are  $c$  fault categories and the coreset size is  $s$ , the ideal probability for each class is  $\frac{c}{s}$ . Thus, we have:

$$\min \lambda \left( \frac{1}{c} \sum_{l=1}^c \left| p_l^t - \frac{c}{s} \right| \right), \quad (8)$$

where  $\lambda$  is a regularization parameter that balances the importance of the class proportion term.  $p_l^t$  is the proportion of samples from class  $l$  in the selected coreset  $S_u^t$ .

Moreover, to handle model updates with insufficient labeled data, a pseudo-labeling strategy can leverage the abundance of unlabeled data. Directly using the model's predicted labels as pseudo-labels is intuitive but can result in mislabeled data, degrading performance. Therefore, generating accurate pseudo-labels is crucial. Let  $v_j^t \leftarrow f(\phi(z_j^t); \theta_{t-1})$  denote the process of generating pseudo-labels. The entire problem of achieving a robust and realistic SRTFD can be formulated as follows:

$$\begin{aligned} \min & \left[ \sum_{j=1}^s \mathcal{L}(f(\phi(z_j^t); \theta_t), v_j^t) - \sum_{k=1}^u \mathcal{L}(f(\phi(x_k^t); \theta_t), y_k^t) \right] \\ & + \lambda \left( \frac{1}{c} \sum_{l=1}^c \left| p_l^t - \frac{c}{s} \right| \right), \quad (9) \\ \text{s.t. } & S^t \cap S^T = \emptyset, \quad T = 1, 2, \dots, t-1, \\ & v_j^t \leftarrow f(\phi(z_j^t); \theta_{t-1}). \end{aligned}$$

## 4 METHODOLOGY

This section introduces the SRTFD framework, illustrated in Figure 1. The prediction and training processes are synchronized, with most data for model updating coming from previously unlabeled data and only a small portion being labeled. This approach is realistic for modern complex systems. The framework consists of three main components: Retrospect Coreset Selection (RCS), Global Balance Technique (GBT), and Confidence and Uncertainty-driven Pseudo-label Learning (CUPL). Each component will be detailed in the following subsections.

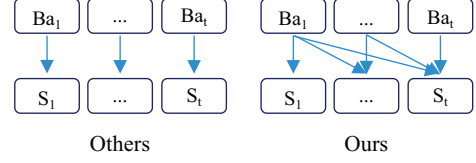


**Figure 2: Comparison of existing [22] and our coreset selection approaches. The  $Ba_t$  and  $S_t$  denote the batch data and selected coreset in  $t$  time, respectively.**

### 4.1 Retrospect Coreset Selection (RCS)

To optimize fault diagnosis (FD) tasks, we introduce Retrospect Coreset Selection (RCS). RCS selects a representative coreset by considering all historical data, and addressing memory constraints through efficient implementation. Specifically, we use the buffer in the system to store samples that encapsulate all historical data, enabling effective RCS. By assessing the similarity between incoming data and buffer data, we eliminate redundancy. When new data arrives, the buffer filters out redundant information, ensuring that coreset selection focuses on novel, non-redundant data. This approach also reduces computational load by bypassing updates when new batches closely resemble existing data.

Given the large-scale nature of the data, directly computing Euclidean distances between new samples and buffer entries is computationally intensive. To mitigate this, we employ batch-wise metrics and cluster the buffer data. Let  $B^t = \{(x_{b_1}^t, y_{b_1}^t), \dots, (x_{b_n}^t, y_{b_n}^t)\}$  represent the buffer at time  $t$ , where  $x_{b_i}^t \in (X^t \cup X_u^t)$  and  $y_{b_i}^t \in (Y^t \cup Y_u^t)$ , with  $i = 1, 2, \dots, bn$ , and  $bn$  being the total number of buffer samples at time  $t$ . Labels  $y_{b_i}^t$  fall within  $\{0, 1, \dots, bc_t\}$ , where  $bc_t$  is the number of classes at time  $t$ . We partition buffer data into  $bc_t$  clusters based on these labels, denoted as  $\{X_{b_1}^t, X_{b_2}^t, \dots, X_{b_{bc_t}}^t\}$ . By clustering the buffer data, we reduce the computational burden, enabling batch-wise comparison instead of individual distance calculations.

For the newly arrived data  $X_u^t$ , we employ the MiniBatchKMeans algorithm [33], a highly efficient clustering method designed for large-scale datasets, to partition the data into different clusters. This algorithm accelerates computation and reduces memory usage by processing data in small batches. By clustering  $X_u^t$  into  $uc$  clusters, denoted as  $\{X_{u_1}^t, X_{u_2}^t, \dots, X_{u_{uc}}^t\}$ , where  $X_{u_i}^t$  represents the  $ui$ -th cluster and  $ui = 0, 1, \dots, uc$ . The number of clusters  $uc$  must be less than or equal to the number of samples in the arriving batch  $un$ , and there is no clustering performed if  $uc$  equals  $un$ . Then, the similarity between  $X_{u_i}^t$  and  $B_{b_i}^t$  can be calculated by Kullback-Leibler (KL) divergence [21], which is denoted as:

$$d_{b_i, u_i}^t = KL(X_{b_i}^t, X_{u_i}^t). \quad (10)$$

If  $d_{b_i, u_i}^t$  is less than a threshold  $\tau$ , the cluster  $X_{u_i}^t$  is considered non-redundant. Then, we have

$$S^t = \left\{ \bigcup_{ui=1}^{uc} X_{u_i}^t \mid d_{b_i, u_i}^t \leq \tau \right\} \quad (11)$$

This buffer retrospective process ensures that only the most informative and non-redundant data points are retained in the coreset. Thus, the goal of  $S_u^t \cap S_u^T = \emptyset$ , for  $T = 1, 2, \dots, t-1$ , is achieved.

Selecting the most representative samples is recognized as an NP-hard problem. However, in the recent OCL technique Camel [22], transformed this challenge into a submodular maximization problem. Building on their work, we iteratively select two samples with the largest Euclidean distance until the coreset size requirement is satisfied. The selection of the coreset  $S^t$  in RCS is defined as follows:

$$S^t = \{Z^t \subseteq \bigcup_{ui=1}^{uc} X_{ui}^t \mid d_{bi,ui}^t \geq \tau, d_{\max}\}, \quad (12)$$

here,  $d_{\max} = \max_{i,j \in [s]} \|z_i - z_j\|$ , with  $z_i, z_j \in Z^t$  and  $s$  being the size of the coreset.  $Z^t$  is a subset of  $\bigcup_{ui=1}^{uc} X_{ui}^t$ . The distance metric  $d_{bi,ui}^t$  ensures that only data points with a similarity measure above a threshold  $\tau$  are selected.  $d_{\max}$  represents the maximum Euclidean distance between any two samples within  $Z^t$ .

## 4.2 Global Balance Technique (GBT)

As highlighted in the introduction, the imbalance problem significantly impacts the performance of fault diagnosis systems. Current online continual learning (OCL) methods rarely address this issue adequately. They typically attempt to mitigate it by selecting a coreset that appears balanced from the current batch data, prioritizing samples from less-represented classes. However, this often results in a pseudo-balanced coreset that does not reflect a truly balanced distribution. For instance, if a class has many samples in the buffer but few in the current batch, existing OCL methods will select more samples from this class, neglecting genuinely under-represented classes. Furthermore, in cases of extreme imbalance, selecting a balanced coreset alone cannot resolve the problem, as the selected coreset often remains unbalanced. Therefore, we propose GBT, which addresses this issue based on two critical factors affecting fault diagnosis performance: the quality of training data and the frequency of model updates.

From the perspective of training data, feeding a balanced dataset into the model will undoubtedly enhance its performance. However, the FD model is trained on both the current batch of data and the data stored in the buffer. Focusing solely on the current batch data makes it easy to obtain a pseudo-balanced coreset. Thus, it is essential to consider both the buffer samples and the categories, and the corresponding objective function (8) becomes:

$$\min \left( \frac{1}{c} \sum_{l=1}^c \left| ps_l^t - \frac{c}{s} \right| \right) + \left( \frac{1}{bc_t} \sum_{l=1}^{bc_t} \left| pb_l^t - \frac{bc_t}{bn} \right| \right) \quad (13)$$

where  $ps_l^t$  and  $pb_l^t$  represent the true probabilities of the  $l$ -th classes in the current coreset and buffer, respectively.  $bn$  represents the total sample size in the buffer, and  $bc_t$  denotes the number of classes in the buffer at  $t$  time. This approach ensures a genuinely balanced dataset by selecting samples from the least represented classes in both the buffer and the current coreset.

From the perspective of model updates, considering the scenario where certain classes have a significantly low number of samples, with  $ps_l^t \ll \frac{c}{s}$  and  $pb_l^t \ll \frac{bc_t}{bn}$ , it becomes evident that selecting a balanced coreset is unfeasible. Therefore, we introduce the following loss function:

$$\mathcal{L} = - \sum_{i=1}^b (1 - p_i)^\gamma \log(p_i) - \sum_{j=1}^s \alpha (1 - p_j)^\gamma \log(p_j) \quad (14)$$

where  $p_i = f_{\theta_t}(x_{bi})$  and  $p_j = f_{\theta_t}(z_j)$  are the predicted probabilities for data from the buffer and coreset, respectively.  $\alpha$  represents the data weights in coreset. The modulating factor  $\gamma$  reduces the loss from easy-to-classify examples, encouraging the model to focus on harder cases. Equation (14) directs the model's attention towards underrepresented and difficult classes, effectively mitigating the class imbalance issue.

## 4.3 Confidence and Uncertainty-driven Pseudo-label Learning (CUPL)

The proposed CUPL module enhances the SRTFD training process by utilizing both labeled and unlabeled data. The critical components of this method include generating pseudo-labels and employing a selection strategy to incorporate these labels into the training set. Here, the pseudo-labels  $v_j$  are determined directly by the maximum probability, expressed as  $v_j = \Gamma[\max(p_j)]$ . For the selection strategy, the conventional approach for selecting pseudo-labeled samples is to choose those with high confidence. However, since most newly arriving data are normal data, the model shows high confidence in predicting these normal instances but low confidence in identifying rare faults. Thus, relying solely on high-confidence selections can degrade overall performance in FD tasks.

Inspired by the work of Mamshad et al. [30], we introduce both positive and negative label selection. Specifically, samples are selected as positive pseudo-labels when the model's predicted probability is high, and as negative pseudo-labels when the probability is extremely low, which can be denoted as follows:

$$g_j = \mathbf{1}[p_j \geq \tau_p] + \mathbf{1}[p_j \leq \tau_n], \quad (15)$$

where  $g_j$  is an indicator that determines whether the sample  $j$  is selected. The indicator function  $\mathbf{1}[\cdot]$  returns 1 if the condition inside the brackets is true and 0 otherwise. The thresholds  $\tau_p$  and  $\tau_n$  are used to select positive and negative pseudo-labels, respectively.

Additionally, it has been demonstrated that predictions with low uncertainty are more likely to result in correct pseudo-labels, as shown by Mamshad's research. Therefore, we incorporate an uncertainty constraint into the positive and negative pseudo-label selection process. The uncertainty of model predictions can be estimated using Monte Carlo dropout (MCDropout) [25]. MCDropout estimates uncertainty by incorporating dropout during the inference phase. The process involves performing multiple stochastic forward passes through the network, each time applying dropout with a certain probability  $p$ . For a layer with output  $\mathbf{h}$ , the output with dropout is  $\mathbf{h}' = \mathbf{h} \odot \mathbf{d}$ , where  $\mathbf{d} \sim \text{Bernoulli}(p)$ . Repeating this process  $T$  times results in a set of predictions  $\{\hat{\mathbf{y}}^{(1)}, \hat{\mathbf{y}}^{(2)}, \dots, \hat{\mathbf{y}}^{(T)}\}$ . The mean prediction is calculated as  $\hat{\mathbf{y}}_{\text{mean}} = \frac{1}{T} \sum_{t=1}^T \hat{\mathbf{y}}^{(t)}$ , and the uncertainty is estimated using the variance  $\hat{\sigma}^2 = \frac{1}{T} \sum_{t=1}^T (\hat{\mathbf{y}}^{(t)} - \hat{\mathbf{y}}_{\text{mean}})^2$ . This approach is simple to implement, requiring no complex modifications to the model architecture, and provides valuable insights into the model's confidence in its predictions, especially with uncertain or complex input data.

By utilizing both the confidence and uncertainty of network predictions, a more accurate subset of pseudo-labels can be selected. The selection function becomes:

$$g_i = 1 [\hat{\sigma}^2 \leq \kappa \text{ and } p_j \geq \tau_p] + 1 [\hat{\sigma}^2 \leq \kappa \text{ and } p_j \leq \tau_n], \quad (16)$$

where  $\kappa$  is the uncertainty thresholds.

## 5 EXPERIMENTS

### 5.1 Experimental Setup

Experiments were conducted on an Intel(R) Xeon(R) w7-3455 system with an NVIDIA RTX 6000 Ada Generation GPU (48GB GDDR6) and 512GB of RAM. The software used includes Python 3.12.4 and PyTorch 2.3.0 with CUDA 12.1.

**Datasets:** Table 2 summarizes the datasets used in our experiments. (1) Hot Roll of Steel (HRS): The hot rolling process in steel manufacturing requires monitoring conveyor rollers to prevent billet deformation, surface defects, downtime, and increased costs. This dataset, from an actual hot rolling steel industry, includes data from 294 rollers recorded via motor current signals and converted to digital data. It encompasses five fault categories: roller swing, roller stuck, overcurrent, squeaking, and base deformation. Due to the random occurrence of these faults, the dataset is highly unbalanced and contains limited samples. (2) Tennessee-Eastman process (TEP): It is widely used to validate fault diagnosis methods. It includes 21 distinct fault categories with training and testing sets. In this study, 4320 normal samples and 800 samples for each fault are used. (3) CAR Learning to Act (CARLA): Yan et al. [39] collected this dataset using Dosovitskiy’s [12] autonomous driving simulator. It features single-sensor and multi-sensor faults across three maps: rainy, cloudy, and sunny conditions. There are 9 categories of single-sensor faults and 4 categories of multi-sensor faults. Each map had a 30-minute simulation with sensor data sampled at 60Hz.

**Testing Scenarios:** We conduct experiments on three datasets under two scenarios: class-incremental and variable working conditions. The proposed method supports online continuous learning, eliminating the need to divide data into training and testing sets. We first initialize the network using 1000 normal samples. As monitoring data arrives, labeled samples and reliable samples with predicted labels from previous tasks are used for model training while predicting the new data. For class-incremental scenarios, normal samples are randomly divided equally into each task, and each fault sample appears in each task in turn. For varying working conditions, only the CARLA dataset includes three conditions, while the HRS and TEP datasets each have one, as shown in Table 2. We gradually introduce noise into the HRS and TEP samples to simulate different working conditions. In the CARLA dataset, monitoring data evolve randomly from condition 1 to condition 2, and then to condition 3.

**Competing Methods:** We selected five methods, including state-of-the-art FD and four advanced OCL approaches, as benchmark algorithms for performance comparison: 1) Baseline: A basic model trained using experience replay (ER) [7], achieving online continuous learning by replaying examples from previous tasks. 2) Adversarial Shapley Value Experience Replay (ASER) [34]: Maintains learning stability and optimizes new class boundaries in the online class-incremental setting. 3) Camel [22]: An advanced OCL method that accelerates model training and improves data efficiency through coresets selection. 4) Averaged Gradient Episodic Memory (AGEM) [6]: Evaluates OCL efficiency in terms of sample complexity, computational cost, and memory usage. 5) MPOS-RVFL [18]: An advanced

ML-based FD method focused on real-time fault diagnosis with imbalanced data.

**Implementations:** The transformer network structure is used for all DL-based benchmarks. The basic neural network consists of an encoder, decoder, transformer encoder as the feature extractor, and a fully connected layer as the predictor. The encoder’s hidden layer dimensions are 500, 500, and 2000, respectively, and the decoder’s dimensions are 2000, 500, and 500. Model training used a learning rate of 0.0001 with the SGD optimizer, a maximum of 200 epochs, and a batch size of 100.

### 5.2 Performance Comparison

Given the imbalanced nature of the experimental datasets, accuracy is not reliable. Therefore, we used metrics specifically designed for imbalanced datasets: Recall, Precision, G-mean, and F1 score. Recall measures the proportion of actual positives correctly identified, while Precision measures the proportion of predicted positives that are correct. G-mean balances sensitivity and specificity, and the F1 score is the harmonic mean of Precision and Recall. We also compared model training time. Our results are averaged across all tasks after the final update, denoted as Avg-End-Rel for Recall, Avg-End-Pre for Precision, Avg-End-Gmean for G-mean, and Avg-End-F1 for F1 score.

**Class-incremental:** The comparison results for class-incremental methods are shown in the left part of Table 4. Our method requires the least training time on all datasets and outperforms other DL-based methods. Although the ML-based method MPOS-RVFL requires less training time, its performance is significantly inferior to other DL methods. The ER method is competitive, outperforming our method by 2.3% in the four metrics on the CARLA-S dataset. However, ER’s training time is 4.56 times longer, at 222.44 seconds compared to our 48.40 seconds. These results highlight the effectiveness of SRTFD in balancing high performance with reasonable training times across various datasets and conditions.

**Variable working conditions:** The right part of Table 4 shows the performance comparison under variable working conditions across three datasets. SRTFD consistently outperforms other approaches, achieving the highest scores in most performance metrics. While the ER method outperforms our method on the CARLS-S dataset, it requires much more training time (ER: 456.87 seconds vs. SRTFD: 95.99 seconds). The CAMEL method maintains the second shortest training time across all datasets, leading on the TEP dataset with 105.18 seconds, 20.26 seconds shorter than SRTFD (125.44 seconds). However, CAMEL’s overall performance is 9.7% lower than SRTFD in other metrics. These results highlight the effectiveness of SRTFD in balancing high performance with reasonable training times across various datasets and conditions.

### 5.3 Ablation Study

To evaluate the contribution of each component in SRTFD, we separately removed the RSC, GBT, and CUFL components and conducted experiments on all datasets. We compared the performance before and after removing each component under class-incremental and variable working conditions. From Table 4, the following three conclusions can be drawn.

Table 2: The description of datasets

Dataset	Normal samples	Number of fault classes	Number of each fault	Dimension	Number of working cond.	Total samples
HRS	36333	5	1783/8114/1533/83/83	120	1	47929
TEP	4320	21	800	52	1	31200
CARLS (single-sensor)	89166	9	2404/1803/2404/2404 /2404/1604/2004/1803/2004	10	3	108000
CARLS (multi-sensor)	100885	4	1604/1604/1503/2404	10	3	108000

Table 3: Performance comparison of the SRTFD and other approaches across three datasets in two scenarios.

Dataset	DL/ML-based	Methods	Class-incremental					Variable working condition				
			Avg-End-Rel	Avg-End-Pre	Avg-End-F1	Avg-End-Gmean	Training-Time (s)	Avg-End-Rel	Avg-End-Pre	Avg-End-F1	Avg-End-Gmean	Training-Time (s)
HRS	ML-based	MPOS-RVFL	0.3533	0.4083	0.3760	0.3784	9.04	0.1269	0.1667	0.1441	0.1454	6.73
		ASER	0.3169	0.3750	0.2986	0.3397	355.35	0.1937	0.5990	0.2320	0.3373	225.72
	DL-based	Camel	0.5795	0.4926	0.5082	0.5327	114.64	0.1520	0.5025	0.2185	0.2762	91.29
		AGEM	0.6032	0.5211	0.5382	0.5592	176.79	0.1468	0.5597	0.2142	0.2866	117.98
		ER	0.5331	0.4594	0.4659	0.4935	144.48	0.1660	0.5468	0.1803	0.2937	93.75
		SRTFD	0.6831	0.5663	0.5881	0.6187	56.17	0.5914	0.5215	0.5365	0.5552	59.42
TEP	ML-based	MPOS-RVFL	0.0992	0.1678	0.1151	0.1228	14.33	0.0093	0.0455	0.0154	0.0205	4.27
		ASER	0.1524	0.0737	0.0857	0.1042	348.72	0.3259	0.3258	0.2985	0.3258	350.97
	DL-based	Camel	0.1619	0.1173	0.1263	0.1359	116.29	0.2364	0.2773	0.2289	0.2559	105.18
		AGEM	0.1534	0.0993	0.1029	0.1208	139.47	0.2975	0.2643	0.2453	0.2803	131.21
		ER	0.1721	0.1471	0.1491	0.1567	121.97	0.3351	0.3509	0.3219	0.3428	127.91
		SRTFD	0.1950	0.1606	0.1572	0.1742	77.10	0.3450	0.3569	0.3358	0.3508	125.44
CARLS-S	ML-based	MPOS-RVFL	0.2694	0.2929	0.2787	0.2804	20.57	0.3755	0.4183	0.3942	0.3955	29.80
		ASER	0.2749	0.2642	0.2179	0.2579	563.18	0.5155	0.4378	0.4366	0.4718	1181.92
	DL-based	Camel	0.3896	0.3657	0.3274	0.3711	156.65	0.5733	0.5025	0.4925	0.5319	357.42
		AGEM	0.4706	0.4501	0.4178	0.4569	271.62	0.6249	0.5031	0.4997	0.5543	560.76
		ER	0.5295	0.5916	0.5077	0.5587	222.44	0.5907	0.5482	0.5550	0.5682	456.87
		SRTFD	0.5519	0.5160	0.4972	0.5306	48.04	0.5982	0.5115	0.5117	0.5521	95.99
CARLS-M	ML-based	MPOS-RVFL	0.4410	0.4567	0.4484	0.4486	29.89	0.4608	0.4833	0.4715	0.4718	28.92
		ASER	0.3701	0.4042	0.2625	0.3723	525.43	0.6985	0.6428	0.6488	0.6679	621.28
	DL-based	Camel	0.5610	0.5303	0.5021	0.5388	148.50	0.5775	0.4836	0.4720	0.5221	230.10
		AGEM	0.5503	0.5183	0.5166	0.5326	262.09	0.6062	0.4068	0.3983	0.4784	355.06
		ER	0.6269	0.6403	0.6172	0.6332	229.13	0.7856	0.6886	0.7109	0.7330	281.76
		SRTFD	0.6108	0.7133	0.6400	0.6568	45.57	0.8223	0.7089	0.7314	0.7617	37.35

Table 4: Performance of SRTFD compared to its variants without each component across three datasets.

Dataset	Methods	Class-incremental					Variable working condition				
		Avg-End-Rel	Avg-End-Pre	Avg-End-F1	Avg-End-Gmean	Training-Time (s)	Avg-End-Rel	Avg-End-Pre	Avg-End-F1	Avg-End-Gmean	Training-Time (s)
HRS	SRTFD w/o RSC	0.6034	0.5619	0.5725	0.5815	362.29	0.7196	0.6808	0.6862	0.6998	307.35
	SRTFD w/o GBT	0.6437	0.5464	0.5699	0.5919	218.17	0.6750	0.7005	0.6858	0.6875	174.93
	SRTFD w/o CUPL	0.5897	0.5003	0.5127	0.5405	56.00	0.4109	0.4311	0.4019	0.4198	18.08
	SRTFD	0.6831	0.5663	0.5881	0.6187	56.17	0.5914	0.5215	0.5365	0.5552	59.42
	SRTFD w/o RSC	0.2174	0.1642	0.1743	0.1880	168.05	0.3203	0.3469	0.3119	0.3332	159.60
TEP	SRTFD w/o GBT	0.2053	0.1889	0.1793	0.1857	140.25	0.2036	0.2105	0.1919	0.2070	115.17
	SRTFD w/o CUPL	0.1055	0.0824	0.0803	0.0915	87.94	0.2343	0.2615	0.2221	0.2474	65.86
	SRTFD	0.1950	0.1606	0.1572	0.1742	77.10	0.3450	0.3569	0.3358	0.3508	125.44
	SRTFD w/o RSC	0.5133	0.5169	0.4769	0.5135	334.64	0.6878	0.5972	0.6133	0.6390	986.64
	SRTFD w/o GBT	0.5922	0.5518	0.5410	0.5702	222.49	0.7340	0.5878	0.6098	0.6526	689.73
CARLS-S	SRTFD w/o CUPL	0.3907	0.4732	0.3684	0.4265	61.42	0.3620	0.3302	0.3221	0.3450	34.19
	SRTFD	0.5519	0.5160	0.4972	0.5306	48.04	0.5982	0.5115	0.5117	0.5521	95.99
	SRTFD w/o RSC	0.6222	0.6360	0.6121	0.6262	673.35	0.7905	0.6881	0.7134	0.7363	300.65
	SRTFD w/o GBT	0.7389	0.7149	0.7176	0.7255	190.73	0.8236	0.6199	0.6379	0.7044	99.53
	SRTFD w/o CUPL	0.5104	0.4865	0.4446	0.4939	55.39	0.7764	0.6644	0.6906	0.7168	44.34
CARLS-M	SRTFD	0.6108	0.7133	0.6400	0.6568	45.57	0.8223	0.7089	0.7314	0.7617	37.35

First, the RSC module effectively reduces model training time. When comparing *SRTFD* with *SRTFD w/o RSC*, the training duration of *SRTFD* is significantly shortened across all datasets while maintaining comparable performance across four metrics. For instance, in the HRS dataset within a class-incremental setting, the training time is reduced by 80.66%, and the Avg-End-rel improves by 13.22%.

Second, the GBT module contributes to reducing model training time and improving FD performance. The GBT module, which considers balanced coreset selection, is integrated with the RSC module responsible for coreset selection. As a result, *SRTFD w/o GBT* performs better than *SRTFD* due to training on more data, but requires more training time. For example, in the TEP dataset

within a class-incremental setting, *SRTFD w/o GBT* increases Avg-End-Rel by 1.03% but decreases training time by 45.26%. However, in the HRS and TEP datasets, and in some cases of the CARLS data, *SRTFD w/o GBT* performs worse than *SRTFD w/o RSC*. For instance, Avg-End-Pre of *SRTFD w/o GBT* is 0.5878, while *SRTFD w/o RSC* is 0.5972. This shows the effectiveness of the GBT module in handling imbalanced data.

Lastly, the CUPL module significantly improves FD performance. While the training time for *SRTFD w/o CUPL* may be shorter in certain cases, it is evident that its performance is markedly inferior to that of *SRTFD*. A comparison between *SRTFD* and *SRTFD w/o CUPL* reveals that the extensive use of pseudo-labeled samples



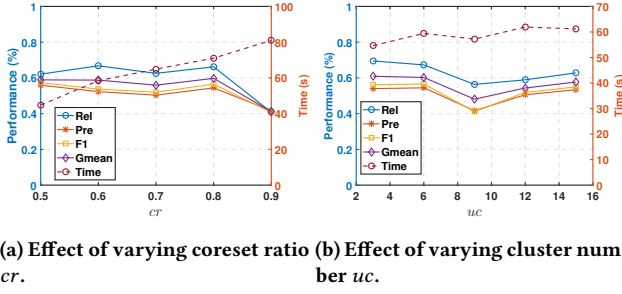


Figure 3: Performance of different coreset ratios  $cr$  and cluster numbers  $uc$  on HRS datasets within class-incremental.

for model training substantially improves FD performance. For instance, the Avg-End-Rel of *RSTFD* increased by 9.34% in the HRS dataset within a class-incremental setting, while the training times are similar (56.17 vs. 56.00 seconds).

## 5.4 Analysis and Discussion

**5.4.1 Effects of coreset ratio and cluster number  $uc$ .** The impact of these two parameters is illustrated in Figure 3 and Figure 5 in the appendix. Panels (a-d) in Figure 5 show the performance across all datasets in the class-incremental scenario for coreset ratios of [0.5, 0.6, 0.7, 0.8, 0.9]. From this figure, it can be observed that as the coreset ratio increases, the number of samples in the coreset grows, leading to longer training times for the model. Additionally, when the coreset ratio is 0.6, the performance of the HRS, CARLS-S, and CARLS-M models is relatively better, and the training time is shorter. Additionally, Figures 5 (e-h) demonstrate the model performance with different numbers of clusters,  $uc$ , set to [3, 6, 9, 12, 15]. From the figures, it can be observed that although the training performance of the models is relatively stable across different  $uc$  values, the choice of  $uc$  is related to the number of categories in the dataset. For instance, the HRS dataset has 5 categories, while the TEP dataset has 22 categories. Therefore, on the HRS dataset, a  $uc$  value of 3 achieves a trade-off in performance across the four metrics and training time, whereas on the TEP dataset, a  $uc$  value of 12 achieves a balance.

**5.4.2 Effects of parameters for pseudo-label samples selection.** For the selection of pseudo-label samples, there are three thresholds, positive label threshold  $\tau_p$ , negative label threshold  $\tau_n$ , and uncertainty threshold of model prediction  $k$ . Figure 4 (a, b, c) and Figure 6 in the appendix demonstrate the performance of these three thresholds on different datasets. Regarding the positive label threshold, as shown in Figures 6 (a-d), higher values lead to better model performance due to using pseudo-labels with higher confidence. For the negative label threshold, as shown in Figure 6 (e-h), a value of 0.45 results in the best performance across all datasets. When the threshold exceeds 0.45, the model performance tends to decline, as illustrated in Figure 6 (f) for the TEP dataset. The impact of the uncertainty threshold on model performance is shown in Figures 6 (i-l). When the value is set to 2, the model performs better across all datasets.

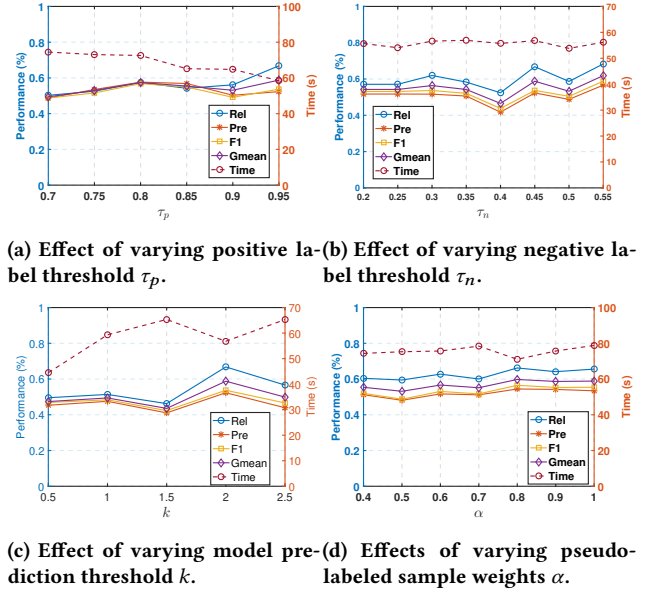


Figure 4: Performance of different thresholds and weights on HRS datasets within class-incremental setting.

**5.4.3 Effects of pseudo-labeled sample weights  $\alpha$ .** Figure 4 (d) and Figure 7 in the appendix show the performance of different pseudo-labeled sample weights  $\alpha$  on all datasets within class-incremental setting. From Figure 7, it can be observed that changes in the value of  $\alpha$  do not significantly impact the model training time. However, there are minor effects on the model's Recall, Precision, F1, and Gmean metrics. The optimal performance is achieved with an  $\alpha$  value of 0.7 on the HRS, TEP, and CARLS-M datasets, while an  $\alpha$  value of 0.6 performs best on the CARLS-S dataset.

## 6 RELATED WORK

**Fault Diagnosis.** Current state-of-the-art fault diagnosis (FD) techniques, summarized in Table 1, fail to meet real-world demands. Modern FD methods must adapt to new fault classes and conditions, handle scalable data, provide real-time responses, and function with minimal prior information, such as limited labeled samples. Despite advances, existing FD methods face significant challenges. For instance, OSELM [19], D-CART [11], and TCNN [38] struggle with data efficiency and scalability. OSSBLS [28] and ODDFD [23] manage limited labeled data but fail to address data imbalance effectively. AMPNet [15] handles large-scale data but lacks adaptability to new fault types and changing environments. Additionally, 1D-CNN [13] faces significant challenges with scalability. OLFA [39] manages limited labeled data but does not effectively address real-time response and high accuracy. Real-time response capabilities are crucial, yet only TCNN [38] shows low training costs conducive to quick responses, unlike AMPNet [15] and OLFA [39]. Effective diagnosis with minimal labeled samples remains a challenge for



many methods. High performance and low training costs are essential but not prioritized by several methods, making them impractical in real-world applications. Thus, there is a critical need for advanced, scalable, and precise FD techniques that address these challenges effectively. In parallel, recent advancements in computer vision have focused on industrial anomaly detection (IAD) [4, 10, 14, 35]. However, existing IAD approaches are unsuitable for FD due to fundamental differences. FD targets specific functional problems using sensor data [15], while IAD identifies statistical features and pattern changes indicating abnormalities using image data [3, 36]. Thus, the clear distinction of use cases drives also a clear separation of concerns.

**Online Continual Learning.** OCL aims to develop models that can continuously learn from a stream of data without forgetting previously acquired knowledge [2]. Key methods include replay-based techniques like experience replay (ER) [7] and adversarial shapley value experience Replay (ASER) [34], which store and replay subsets of past data. Regularization approaches such as gradient episodic memory (GEM) [24] and averaged GEM (AGEM) [6] add constraints to protect important weights. Parameter isolation methods like progressive neural networks [32] and PackNet [26], allocate different model parameters to different tasks. Coreset selection methods like GoodCore [5] and Camel [22], further address scalability and memory efficiency issues of OCL by selecting representative data subsets. While OCL provides a robust framework, it requires significant adaptation to effectively meet the unique demands of real-time fault diagnosis in modern industrial environments.

## 7 CONCLUSION

This paper addresses high training costs, limited labeled samples, and imbalance issues in scalable real-time fault diagnosis using online continual learning with coreset selection. The proposed SRTFD framework comprises three key components: *RCS*, *GBT*, and *CUPL*. These innovations enhance fault diagnosis by improving model performance and efficiency in industrial settings. Extensive validation on real-world and simulated datasets shows significant improvements in four metrics while reducing training time. Our approach tackles data redundancy and imbalance, providing cost-efficient and robust solutions for industrial fault diagnosis. Future work will optimize the SRTFD framework and explore its applicability to other industrial processes and environments.

## REFERENCES

- [1] Anam Abid, Muhammad Tahir Khan, and Javaid Iqbal. 2021. A review on fault detection and diagnosis techniques: basics and beyond. *Artificial Intelligence Review* 54, 5 (2021), 3639–3664.
- [2] Rahaf Aljundi, Eugene Belilovsky, Tinne Tuytelaars, Laurent Charlin, Massimo Caccia, Min Lin, and Lucas Page-Caccia. 2019. Online continual learning with maximal interfered retrieval. *Advances in neural information processing systems* 32 (2019).
- [3] Jaehyeok Bae, Jae-Han Lee, and Seyun Kim. 2023. PNI: Industrial anomaly detection using position and neighborhood information. In *Proceedings of the IEEE/CVF International Conference on Computer Vision*. 6373–6383.
- [4] Aimira Baitieva, David Hurych, Victor Besnier, and Olivier Bernard. 2024. Supervised Anomaly Detection for Complex Industrial Images. In *Proceedings of the IEEE/CVF Conference on Computer Vision and Pattern Recognition*. 17754–17762.
- [5] Chengliang Chai, Jiabin Liu, Nan Tang, Ju Fan, Dongjing Miao, Jiayi Wang, Yuyu Luo, and Guoliang Li. 2023. GoodCore: Data-effective and Data-efficient Machine Learning through Coreset Selection over Incomplete Data. *Proceedings of the ACM on Management of Data* 1, 2 (2023), 1–27.
- [6] Arslan Chaudhry, Marc’Aurelio Ranzato, Marcus Rohrbach, and Mohamed Elhoseiny. 2018. Efficient lifelong learning with a-gem. *arXiv preprint arXiv:1812.00420* (2018).
- [7] Arslan Chaudhry, Marcus Rohrbach, Mohamed Elhoseiny, Thalaiyasingam Ajanthan, Puneet K Dokania, Philip HS Torr, and Marc’Aurelio Ranzato. 2019. On tiny episodic memories in continual learning. *arXiv preprint arXiv:1902.10486* (2019).
- [8] Hongtian Chen, Bin Jiang, Steven X Ding, and Biao Huang. 2020. Data-driven fault diagnosis for traction systems in high-speed trains: A survey, challenges, and perspectives. *IEEE Transactions on Intelligent Transportation Systems* 23, 3 (2020), 1700–1716.
- [9] Xiaohan Chen, Rui Yang, Yihao Xue, Mengjie Huang, Roberto Ferrero, and Zidong Wang. 2023. Deep transfer learning for bearing fault diagnosis: A systematic review since 2016. *IEEE Transactions on Instrumentation and Measurement* 72 (2023), 1–21.
- [10] Alex Costanzino, Pierluigi Zama Ramirez, Giuseppe Lisanti, and Luigi Di Stefano. 2024. Multimodal industrial anomaly detection by crossmodal feature mapping. In *Proceedings of the IEEE/CVF Conference on Computer Vision and Pattern Recognition*. 17234–17243.
- [11] Huaxia Deng, Yifan Diao, Wei Wu, Jin Zhang, Mengchao Ma, and Xiang Zhong. 2020. A high-speed D-CART online fault diagnosis algorithm for rotor systems. *Applied Intelligence* 50 (2020), 29–41.
- [12] Alexey Dosovitskiy, German Ros, Felipe Codevilla, Antonio Lopez, and Vladlen Koltun. 2017. CARLA: An open urban driving simulator. In *Conference on robot learning*. PMLR, 1–16.
- [13] Mahmoud Elsis, Minh-Quang Tran, Karar Mahmoud, Diaa-Eldin A Mansour, Matti Lehtonen, and Mohamed MF Darwish. 2022. Effective IoT-based deep learning platform for online fault diagnosis of power transformers against cyberattacks and data uncertainties. *Measurement* 190 (2022), 110686.
- [14] Zheng Fang, Xiaoyang Wang, Haocheng Li, Jiejie Liu, Qiugui Hu, and Jimin Xiao. 2023. Fastrecon: Few-shot industrial anomaly detection via fast feature reconstruction. In *Proceedings of the IEEE/CVF International Conference on Computer Vision*. 17481–17490.
- [15] Dennis Fedorishin, Justas Birgiolas, Deen Dayal Mohan, Livio Forte, Philip Schneider, Srirangaraj Setlur, and Venu Govindaraju. 2022. Large-Scale Acoustic Automobile Fault Detection: Diagnosing Engines Through Sound. In *Proceedings of the 28th ACM SIGKDD Conference on Knowledge Discovery and Data Mining*. 2871–2881.
- [16] Zhiwei Gao, Carlo Cecati, and Steven X Ding. 2015. A survey of fault diagnosis and fault-tolerant techniques—Part I: Fault diagnosis with model-based and signal-based approaches. *IEEE transactions on industrial electronics* 62, 6 (2015), 3757–3767.
- [17] Yasir Ghunaim, Adel Bibi, Kumail Alhamoud, Motasem Alfarra, Hasan Abed Al Kader Hammoud, Ameya Prabhu, Philip HS Torr, and Bernard Ghanem. 2023. Real-time evaluation in online continual learning: A new hope. In *Proceedings of the IEEE/CVF Conference on Computer Vision and Pattern Recognition*. 11888–11897.
- [18] Pengyu Han, Shijin Chen, Zeyi Liu, and Xiao He. 2024. Imbalanced Real-time Fault Diagnosis Based on Minority-Prioritized Online Semi-supervised Random Vector Functional Link Network. *IEEE Transactions on Instrumentation and Measurement* (2024).
- [19] Wei Hao and Feng Liu. 2020. Imbalanced data fault diagnosis based on an evolutionary online sequential extreme learning machine. *Symmetry* 12, 8 (2020), 1204.
- [20] Luhao Jin, Yao Mao, Xueqing Wang, Linlin Lu, and Zheng Wang. 2023. Online data-driven fault diagnosis of dual three-phase PMSM drives considering limited labeled samples. *IEEE Transactions on Industrial Electronics* (2023).
- [21] Solomon Kullback and Richard A Leibler. 1951. On information and sufficiency. *The annals of mathematical statistics* 22, 1 (1951), 79–86.
- [22] Yiming Li, Yanyan Shen, and Lei Chen. 2022. Camel: Managing data for efficient stream learning. In *Proceedings of the 2022 International Conference on Management of Data*. 1271–1285.
- [23] Jiahao Lin, Moufa Guo, Qiteng Hong, and Run Jiang. 2024. An earth fault diagnosis method based on online dynamically calculated thresholds for resonant ground systems. *IEEE Transactions on Smart Grid* (2024).
- [24] David Lopez-Paz and Marc’Aurelio Ranzato. 2017. Gradient episodic memory for continual learning. *Advances in neural information processing systems* 30 (2017).
- [25] Liangping Ma and John Kaewell. 2020. Fast Monte Carlo dropout and error correction for radio transmitter classification. In *2020 IEEE International Workshop on Information Forensics and Security (WIFS)*. IEEE, 1–5.
- [26] Arun Mallya and Svetlana Lazebnik. 2018. Packnet: Adding multiple tasks to a single network by iterative pruning. In *Proceedings of the IEEE conference on Computer Vision and Pattern Recognition*. 7765–7773.
- [27] Cen Nan, Faisal Khan, and M Tariq Iqbal. 2008. Real-time fault diagnosis using knowledge-based expert system. *Process safety and environmental protection* 86, 1 (2008), 55–71.
- [28] Xiaokun Pu and Chunguang Li. 2021. Online semisupervised broad learning system for industrial fault diagnosis. *IEEE transactions on industrial informatics* 17, 10 (2021), 6644–6654.

- [29] Yuwei Ren, Aiping Wang, and Hong Wang. 2014. Fault diagnosis and tolerant control for discrete stochastic distribution collaborative control systems. *IEEE Transactions on Systems, Man, and Cybernetics: Systems* 45, 3 (2014), 462–471.
- [30] Mamshad Nayeem Rizve, Kevin Duarte, Yogesh S Rawat, and Mubarak Shah. 2021. In defense of pseudo-labeling: An uncertainty-aware pseudo-label selection framework for semi-supervised learning. *arXiv preprint arXiv:2101.06329* (2021).
- [31] Sebastian Ruder. 2016. An overview of gradient descent optimization algorithms. *arXiv preprint arXiv:1609.04747* (2016).
- [32] Andrei A Rusu, Neil C Rabinowitz, Guillaume Desjardins, Hubert Soyer, James Kirkpatrick, Koray Kavukcuoglu, Razvan Pascanu, and Raia Hadsell. 2016. Progressive neural networks. *arXiv preprint arXiv:1606.04671* (2016).
- [33] David Sculley. 2010. Web-scale k-means clustering. In *Proceedings of the 19th international conference on World wide web*. 1177–1178.
- [34] Dongsub Shim, Zheda Mai, Jihwan Jeong, Scott Sanner, Hyunwoo Kim, and Jongseong Jang. 2021. Online class-incremental continual learning with adversarial shapley value. In *Proceedings of the AAAI Conference on Artificial Intelligence*, Vol. 35. 9630–9638.
- [35] Chengjie Wang, Wenbing Zhu, Bin-Bin Gao, Zhenye Gan, Jiangning Zhang, Zhihao Gu, Shuguang Qian, Mingang Chen, and Lizhuang Ma. 2024. Real-ia: A real-world multi-view dataset for benchmarking versatile industrial anomaly detection. In *Proceedings of the IEEE/CVF Conference on Computer Vision and Pattern Recognition*. 22883–22892.
- [36] Yue Wang, Jinlong Peng, Jiangning Zhang, Ran Yi, Yabiao Wang, and Chengjie Wang. 2023. Multimodal industrial anomaly detection via hybrid fusion. In *Proceedings of the IEEE/CVF Conference on Computer Vision and Pattern Recognition*. 8032–8041.
- [37] Ping Wu, Siwei Lou, Xujie Zhang, Jiajun He, Yichao Liu, and Jinfeng Gao. 2020. Data-driven fault diagnosis using deep canonical variate analysis and Fisher discriminant analysis. *IEEE Transactions on Industrial Informatics* 17, 5 (2020), 3324–3334.
- [38] Gaowei Xu, Min Liu, Zhuofu Jiang, Weiming Shen, and Chenxi Huang. 2020. Online Fault Diagnosis Method Based on Transfer Convolutional Neural Networks. *IEEE TRANSACTIONS ON INSTRUMENTATION AND MEASUREMENT* 69, 2 (FEB 2020), 509–520.
- [39] Xuyang Yan, Mrinmoy Sarkar, Benjamin Lartey, Biniam Gebru, Abdollah Homai-far, Ali Karimoddini, and Edward Tunstel. 2023. An online learning framework for sensor fault diagnosis analysis in autonomous cars. *IEEE Transactions on Intelligent Transportation Systems* (2023).
- [40] Yuxuan Zhou, Yining Dong, and Gang Tang. 2022. Time-varying online transfer learning for intelligent bearing fault diagnosis with incomplete unlabeled target data. *IEEE Transactions on Industrial Informatics* 19, 6 (2022), 7733–7741.
- [41] Junjun Zhu, Quansheng Jiang, Yehu Shen, Chenhui Qian, Fengyu Xu, and Qixin Zhu. 2022. Application of recurrent neural network to mechanical fault diagnosis: A review. *Journal of Mechanical Science and Technology* 36, 2 (2022), 527–542.

## A REPRODUCIBILITY

### 1. Environment Requirements

Ensure you have all the necessary Python packages by installing them from the provided ‘requirements.txt’ file.

### 2. Data Sources

- HRS Dataset: This dataset is private and specific to the requirements of cooperative factories.

- TEP and CARLS Datasets: These two datasets are included in our publicly available code.

### 3. Setting Up and Running SRTFD

#### i. Install Required Packages

Make sure you have Python installed. Then, navigate to the project directory and install the required packages using the following command: `pip install -r requirements.txt`

#### ii. Run SRTFD

Execute the main script to start the SRTFD process:

```
python3 general_main.py -data TEP -num_tasks 22 -cl_type
nc -agent SRTFD -num_runs 1 -N 1000
python3 general_main.py -data TEP -num_tasks 22 -cl_type
vc -agent SRTFD -num_runs 1 -N 1000
python3 general_main.py -data CARLS_S -num_tasks 10 -cl_type
nc -agent SRTFD -num_runs 1 -N 1000
python3 general_main.py -data CARLS_S -num_tasks 10 -cl_type
vc -agent SRTFD -num_runs 1 -N 1000
python3 general_main.py -data CARLS_M -num_tasks 5 -cl_type
nc -agent SRTFD -num_runs 1 -N 1000
python3 general_main.py -data CARLS_M -num_tasks 5 -cl_type
vc -agent SRTFD -num_runs 1 -N 1000
```

Additional Resources For more detailed instructions and documentation, please refer to the project’s test.bash file or the official documentation provided with the project.

## B MORE EXPERIMENTAL RESULTS

The detailed results of the parameter sensitivity analysis on all datasets are shown in Figures 5, 6, and 7.

## C LIMITATIONS

The limitations of the proposed SRTFD mainly include the following three points:

1. Memory Constraints: Retrospect Coreset Selection (RCS) necessitates the storage of historical data, which can lead to substantial memory usage. Efficiently managing this data without compromising performance remains a significant challenge, particularly in long-term deployments.

2. Dependency on Consistent Data Streams: The effectiveness of Stream-based Real-Time Fault Detection (SRTFD) is highly dependent on a continuous and consistent stream of data for ongoing learning and adaptation. Any interruptions or inconsistencies in the data flow can adversely affect the model’s performance and its ability to accurately diagnose faults.

3. Scalability to Diverse Industrial Applications: Although SRTFD is designed to be scalable, adapting the framework to different industrial applications—each with varying types of equipment, fault conditions, and operational environments—may require significant customization. This need for extensive adaptation can limit the

framework's generalizability and ease of implementation across diverse industries.

## D PSEUDO-CODE

The pseudocode of the proposed SRTFD is shown in Algorithm 1.

---

### Algorithm 1 SRTFD Algorithm

---

**Initialization:** Initialize the network  $f_{\theta_0}$

**Input:** Labeled data  $D^t = \{X^t, Y^t\}$  and arrive data  $X_u^t$

- 1). Generated Pseudo-labeled samples by CUPL module
  - 1.1 Predict the label  $Y^t$  by  $f_{\theta_{t-1}}$ , compute the probabil-

ity

for  $X_u^t$ , and the predict uncertainty by variance  $\hat{\sigma}^2$

- 1.2 Generated the Pseudo-labeled dataset by Eq. (16)

- 2). Select coreset  $S^t$  by RSC and GBT modules

- 2.1 Filter redundancy data by Eq.(11)

- 2.2 Select coreset  $S^t$  by using Eq. (12) and Eq. (13)

- 3). Update model  $f_{\theta_t}$

- 3.1 updating model  $f_{\theta_t}$  by using  $S^t, D^t, B^t, \theta_{t-1}$ ,  
Eq. (14) and Eq. (6)

**Output:** Predict  $Y_u^t$  for  $X_u^t$  and update model  $f_{\theta_t}$

---

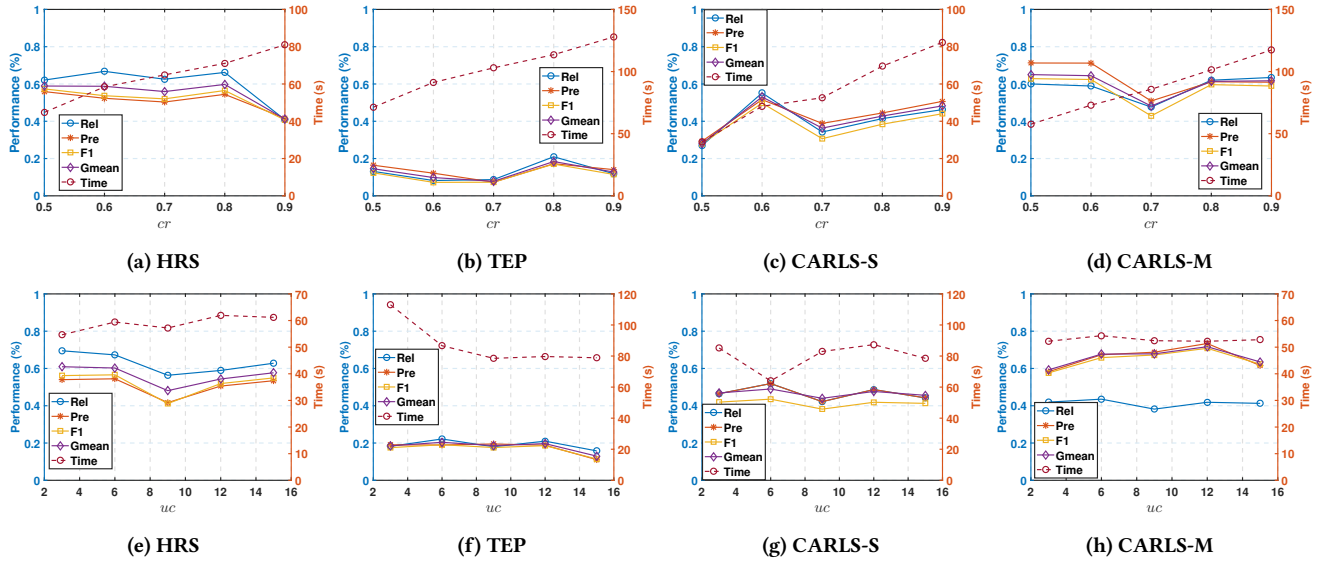
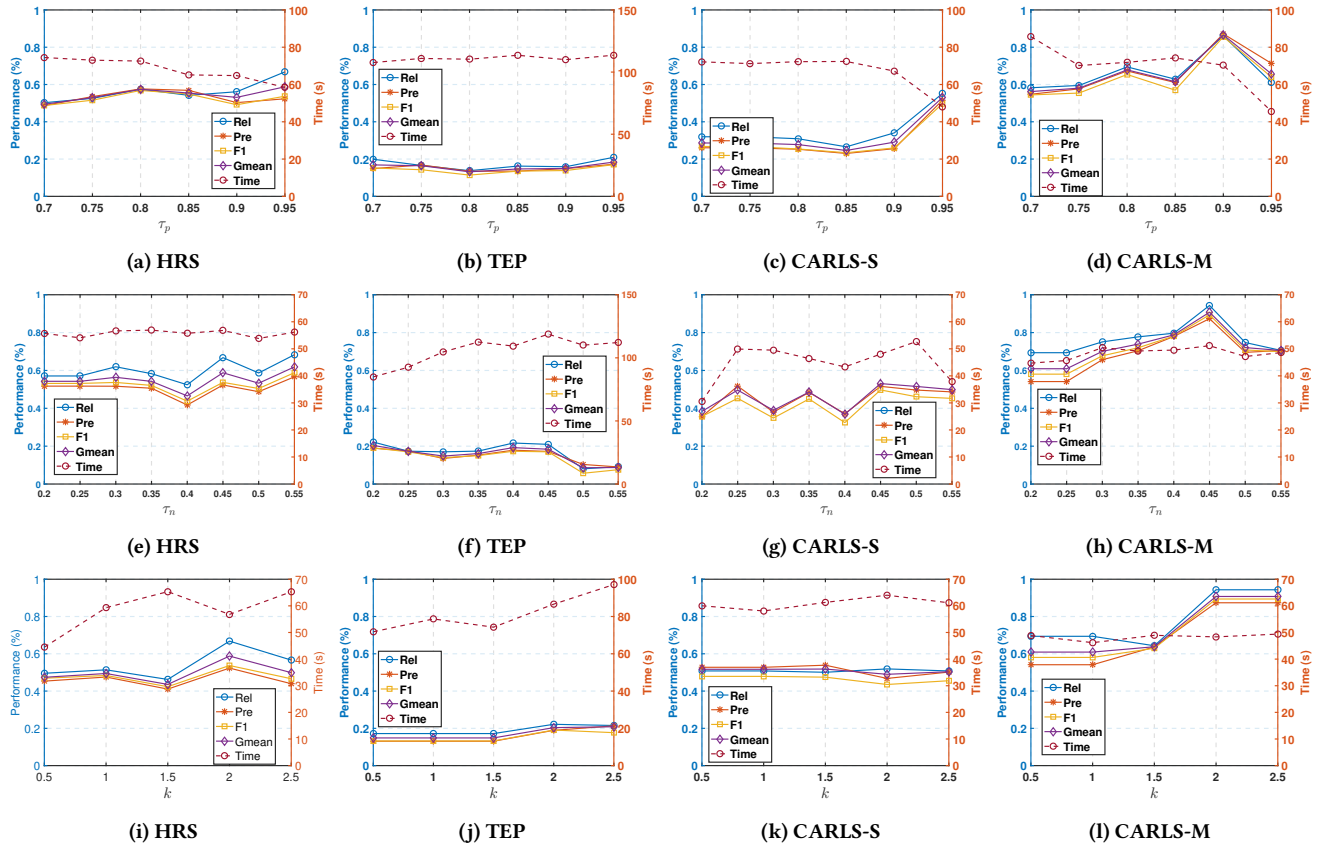
Figure 5: Performance of different coresot ratios and cluster numbers  $uc$  on all datasets within class-incremental.

Figure 6: Performance of different thresholds on all datasets within class-incremental setting.

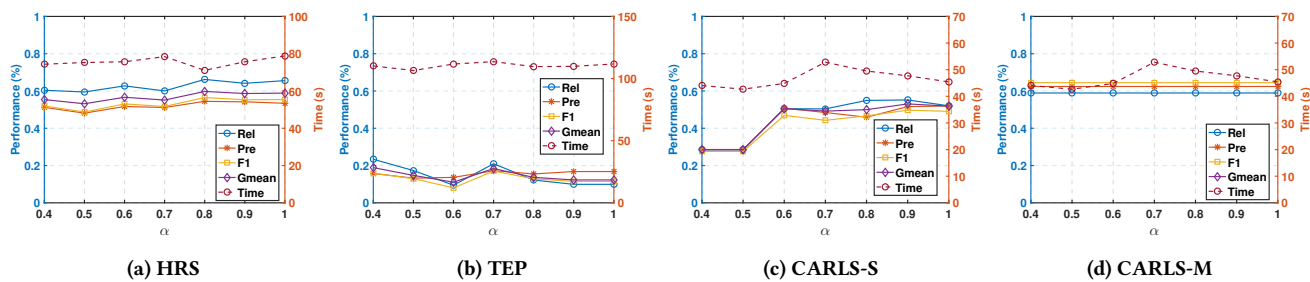


Figure 7: Performance of different weights  $\alpha$  of pseudo-labeled data on all datasets in class-incremental setting.